Modeling of cold mix asphalt evolutive behaviour based on nonlinear viscoelastic spectral decomposition

Marion Lambert, Jean-Michel Piau, Vincent Gaudefroy, Anne Millien, Frédéric Dubois, Christophe Petit, François Chaignon

Manuscript published in Construction and Building Materials, 173 (2018), pp.403-410. Elsevier
https://doi.org/10.1016/j.conbuildmat.2018.03.207

Modeling of cold mix asphalt evolutive behaviour based on nonlinear viscoelastic spectral decomposition

Marion Lambert[a,b,c], Jean-Michel Piau[b], Vincent Gaudefroy[b], Anne Millien[c], Frédéric Dubois[c], Christophe Petit[c], François Chaignon[a]

marion.lambert@ifsttar.fr, jean-michel.piau@ifsttar.fr, vincent.gaudefroy@ifsttar.fr, anne.millien@unilim.fr, frederic.dubois@unilim.fr, christophe.petit@unilim.fr, francois.chaignon@colas.com

a Routes de France, 75008 Paris, France; b LUNAM Université, IFSTTAR MAST, Routes de Bouaye CS4, 44344 Bouguenais, France; c Université de Limoges, GC2D, 19300 Egletons, France

Corresponding author: Christophe Petit - e-mail: christophe.petit@unilim.fr;

Tel: +33 (0)5 55 93 45 19; Fax: +33 (0)5 55 93 45 01

HIGHLIGHTS

- Develop an evolutive constitutive model for cold mixes treated with bitumen emulsion;
- Develop an oedometric test to study the cold mix asphalt evolutive behaviour.

ABSTRACT

Given a political context in which energy and environmental stakes have become increasingly dominant, road engineering practices have favoured saving energy and protecting the environment. Among these practices, the use of cold mixes treated with bitumen emulsion has proven to be a suitable technique. Cold mix design, as well as the design of pavements including cold mix asphalt (CMA) layers, is highly empirical and based on local skills and tend to limit the development of this environmentally-friendly pavement technique. In the case of CMA, no mechanical behaviour law has been established to take into account its evolutive behaviour.

The paper is set in three parts. The CMA model is presented in Part I. The second part of the paper illustrates the numerical response of the model on a compressive sinusoidal load. The last part presents some first simulations of the cyclic oedometer laboratory tests. By comparing then to the numerical simulations, they show the relevance of the model to account for the CMA behaviour.

Keywords: emulsified bitumen, mechanical behaviour, oedometer test, cold mix asphalt.

1. Introduction

Given a political context in which energy and environmental stakes have become predominant, road engineering practices have favored saving energy and protecting the environment [1]. Among these practices, the use of cold mixes treated with bitumen emulsion has proven to be a suitable technique. The design of pavements including cold mix asphalt (CMA) layers [2] however remains highly empirical and based on local skills. From prior experience, the transposition of established local rules from one site to another and their application to pavements subjected to medium or heavy traffic are not simple steps and tend to limit the development of this environmentally-friendly pavement technique. With this objective in mind, a French project with partners from industry and academia was launched a few years ago to promote the use of sustainable road techniques, among which CMA, through defining a rational and coherent CMA pavement design method and finding ways to expand its scope to higher traffic volumes than those typically encountered by this type of material.

CMA displays an evolutive behaviour [3], [4], [5], due to the use of a bitumen emulsion (i.e. mixture of water and bitumen) as binder. In the laboratory, the breaking of the bitumen emulsion and water release are both observed under gyratory compaction [6]. These phenomena are found to be highly correlated with the emulsion formulation,

which must be adapted to the choice of aggregate. In pavements, after compaction the CMA continues to evolve according of the remained water content in the material, in exhibiting a behaviour that remains poorly understood [7]. In the fresh state, CMA behaves like soft and quasi-unbound granular materials. Over time, the material becomes increasingly stiffer with a mechanical behaviour resembling that of a bound asphalt concrete material. The time required to achieve this stiffer mechanical state is called "curing time".

The objective of this paper is to develop a generic curing model for CMA, derived from "merging" the Boyce nonlinear elastic (NLE) model [8], which reflects the behaviour of unbound granular materials at a very early age, with the Huet model [9], which reflects the thermo-viscoelastic behaviour (VE) of hot mix asphalt (HMA) by means of a "curing function". The obtained nonlinear viscoelastic model (NLVE) is based on the use of spectral decomposition for both NLE and VE components. The paper is set in three parts. The CMA model is presented in Part I. The second one of the paper illustrates the numerical response of the model on a compressive sinusoidal load. The last part presents some first simulations of the cyclic oedometer laboratory tests undertaken in parallel to this modelling work.

2. Development of a model to account of the NLVE and curing behaviour of CMA

To design a pavement structure, the first step consists of computing the strain and stress fields generated by the action of traffic loads. Those ones must then be compared with the long-term performances of materials under cyclic mechanical loadings (fatigue tests, cracking tests …) and climatic conditions in relation with the specified pavement life.

The CMA model proposed herein is related to the first step.

~~1.1.~~2.1. Two generic models to describe the behaviour of the CMA in fresh and cured states

Our objective is to develop a generic curing model of CMA, whose behaviour varies from an unbound granular material at a very early age to the thermo-viscoelasticity of asphalt mixes over the long term. To fulfil this objective, two well-known models are firstly considered. One is the Boyce nonlinear elastic (NLE) model for characterising unbound granular materials, while the second is the Huet viscoelastic (VE) model known for its accurate description of HMA.

~~1.1.1.~~2.1.1. Boyce model (3D)

The Boyce's model is a nonlinear extension of Hooke's Law and is based on the hardening dependence with stress of the compressibility K_B and shear G_B moduli, which is typical of the reversible behaviour of unbound granular materials [8]. Using the standard signs and notations of continuum mechanics (contraction strain < 0, compressive stress < 0), the model is written in 3D:

$$\varepsilon_{vol} = -\frac{p}{K_B} \quad (1)$$

$$\varepsilon_q = \frac{q}{3\,G_B} \quad (2)$$

$$\text{with: } K_B = K_a \frac{\left(\frac{p}{Pa}\right)^{1-n}}{1-\gamma\left(\frac{q}{p}\right)^2} \quad (3)$$

$$\text{and: } G_B = G_a \left(\frac{p}{Pa}\right)^{1-n} \quad (4)$$

where:

- $p = -\frac{1}{3}tr(\sigma)$: is the mean pressure;
- $q = \sqrt{\frac{3}{2}tr(s^2)}$: is the deviatoric stress with $s = \sigma + -\frac{1}{3}tr(\sigma)I$ (σ, s = stress and deviatoric stress tensors, I = unit 3x3 tensor);
- $\varepsilon_{vol} = tr(\varepsilon)$: is the volumetric strain;
- $\varepsilon_q = \sqrt{\frac{2}{3}tr(e^2)}$: is the deviatoric strain with $e = \varepsilon - \frac{1}{3}tr(\varepsilon)I$ (ε, e = strain and deviatoric strain tensors);
- P_a, K_a, G_a, γ are positive parameters;

- n is an exponent lying between 0 and 1.

As an example, figures 1 and 2 show the modelling of a cyclic oedometric triaxial test with Boyce model.

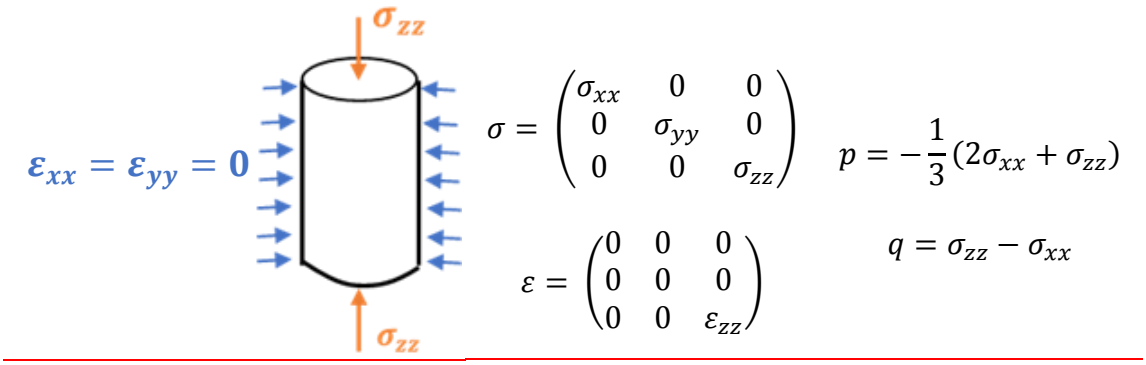

Figure 1. Illustration an oedometric triaxial test

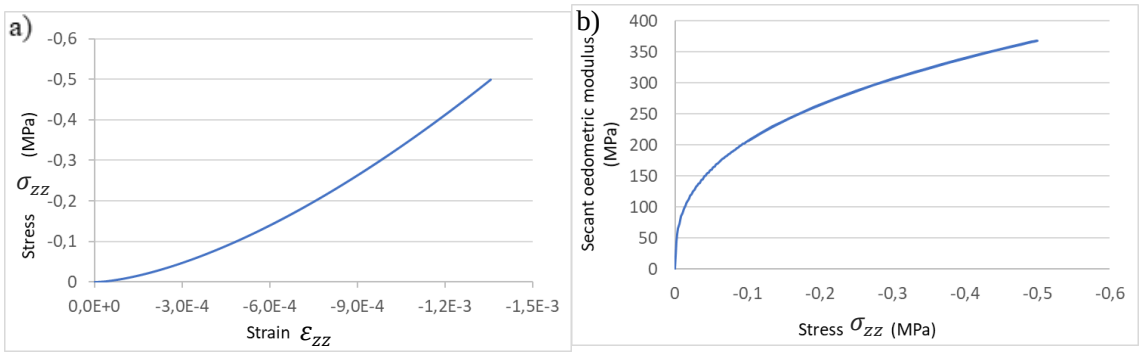

Figure 2. Illustration of Boyce model response in the case of an oedometric triaxial test, a) Stress *vs* strain hardening curve, b) Secant oedometric modulus *vs* axial stress σ_{zz}

~~1.1.2.~~2.1.2. Huet model (1D)

The thermo-viscoelastic model as defined by Huet is composed of a series of elements: one spring E_∞ and two parabolic dashpots (h and k) (fig. 3).

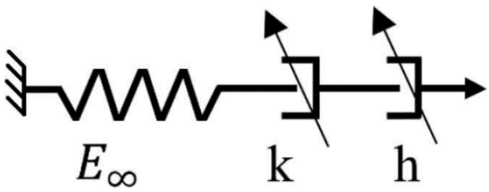

Figure 3. Representation of the Huet model

The complex modulus $\left(E_H^*(\omega)\right)$ and creep function $\left(F_H(t)\right)$ of the Huet model are expressed as:

$$E_H^*(\omega) = \frac{E_\infty}{1+\delta(i\omega a(\theta))^{-k}+(i\omega a(\theta))^{-h}} \quad (5)$$

$$F_H(t) = \frac{1}{E_\infty}\left(1 + \frac{\delta}{\Gamma(k+1)}\left(\frac{t}{a(\theta)}\right)^k + \frac{1}{\Gamma(h+1)}\left(\frac{t}{a(\theta)}\right)^h\right)H(t) \quad (6)$$

where E_∞ is the elastic modulus, h, k are the exponents of parabolic dashpots lying between 0 and 1, δ is the weight of dashpot (k) (positive value), Γ is the Euler function, $a(\theta)$ is the function whose time dimension accounts for the dependence of the material behaviour on temperature θ (decreasing exponential type). $H(t)$ is the Heavyside function.

The relationship between stress and strain can be derived from the creep function by the usual time convolution equation:

$$\varepsilon = F_H \otimes \dot{\sigma} = \int_{-\infty}^{+\infty} F_H(t-u)\frac{d\sigma}{dt}(u)du \quad (7)$$

~~1.1.3.~~2.1.3. Idea basis for the NLE + VE generic laws

At the end our aim is to develop a 3D NLVE constitutive law to account for the real CMA behaviour by mixing NLE component of Boyce's type with VE component of Huet's type; this, in order to be able to compute strain stress fields in pavements submitted to traffic loads and to develop pavement design methodology. However, in this paper, we only present the first step of construction of the constitutive model in 1D that can be generalized in 3D latter on. For our purpose, we then use the 1D following approximations of the laws presented in part 2.1.1 and 2.1.2 that is:

$$\sigma = -E_s(-\varepsilon)^\alpha \quad (8)$$

$$F(t) = B\left(\frac{t}{A}\right)^\beta \text{ with } 0 < \beta < 1 \quad (9)$$

Equation (8) can be derived from Boyce model, using the relationship between the mean pressure and the volumetric strain. Indeed, from equations (1) and (3), one obtains:

$$p = P_a \left(\frac{K_a}{P_a}\right)^{\frac{1}{n}} (-\varepsilon_{vol})^{\frac{1}{n}} \quad (10)$$

which is similar to equation (8) after a change of notation and with $\alpha = \frac{1}{n}$, thus $\alpha > 1$ and with $E_s = P_a \left(\frac{K_a}{P_a}\right)^{\frac{1}{n}}$, having the dimension of an elastic modulus.

Equation (9) is the creep function corresponding to a single parabolic dashpot (fig. 4) considered as sufficient as generic model to describe the viscoelastic behaviour of CMA. β value can be assumed to be close to Huet h exponent, representative of the HMA behaviour for relatively low values of stiffness (at low frequency or at high temperature) which corresponds to the case of CMA.

The A parameter accounts later on for the dependence of the viscosity of CMA both with the age of the material since its manufacturing and with its actual temperature $\theta(t)$. The evolution of this parameter both with curing and $\theta(t)$ is discussed further on in 2.2.4.

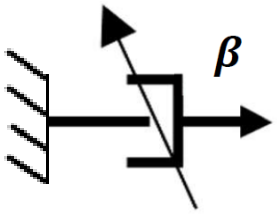

Figure 4. Single parabolic dashpot used as the viscoelastic component of the CMA model

Without restricting the model, B can be taken equal to $\frac{1}{E_s}$ (see equation (8)), just changing A~~(t, {θ})~~ by a multiplicative constant.

In the following, we principally focus on the compressive behaviour of CMA which is the expected response of the material in pavement at young age. But the model that we

present can also account for tensile stresses that may also arise on site after a certain curing time.

~~1.2.~~2.2. Derivation of the CMA model from the spectral decomposition of the two-previous generic NLE and VE laws

It is proposed herein to derive the CMA model from a "juxtaposition" of the two previous equations (8) and (9), by assigning greater weight to the viscoelastic behaviour over time due to parameter A~~$(t,\{\theta\})$~~ increasing with the material age. To carry out the "juxtaposition" of equations (8) and (9) without duplicating the elastic behaviour displayed by both, the two laws are decomposed in spectrum series. The same non-dimensional real variable l, ranging from 0 to $+\infty$, is initially used to continuously index the spectral elements of the two series. In denoting $\varepsilon_l(\sigma, l)$ as the strain distribution over the set of elements, the material strain obtained for such a spectrum can be expressed as:

$$\varepsilon(\sigma) = \int_0^{+\infty} \varepsilon_l(\sigma, l)dl \qquad (11)$$

~~1.2.1.~~2.2.1. Description of the NLE law (8) using a series of "linear spring + mechanical stop" elements

The spectral decomposition of the NLE law, is based on a series of elements l (with $l \in \mathbb{R}^+$) with two branches, a linear spring and a mechanical stop in the compressive domain (fig. 5). The spring value is assumed to be constant across the set of elements and taken equal to the value of parameter E_s in equation (8). The mechanical stops are characterized by their "initial opening value" $b(l)$ considered as positive and which can be presumed without restriction as a decreasing, monotonous function of l (figure 6).

Under compressive stress, the opening of the mechanical stops will decrease until possibly getting shut for the elements which strain is equal to $b(l)$. Then closing elements one after the other leads to the progressive stiffening of the series.

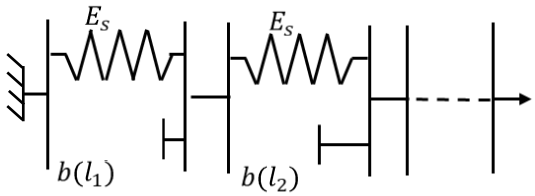

Figure 5. Spectral decomposition for NLE

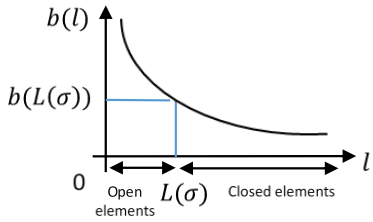

Figure 6. Evolution of the variable $b(l)$

The function $b(l)$ can be defined for any given NLE law σ(ε) (computation given in appendix A). The following function is obtained in the case of equation (8):

$b(l) = \frac{1}{(\alpha\, l)^{\frac{\alpha}{\alpha-1}}}$ which satisfies the requisite assumptions for $\alpha > 1$ (12)

~~1.2.2.~~2.2.2. Representation of equation (9) by its spectral creep series

This type of representation is usual; it may be based on a series of Kelvin-Voigt elements, for which the elastic modulus E is set as a constant whereas the viscosity $\eta(l)$ varies with l (fig. 7).

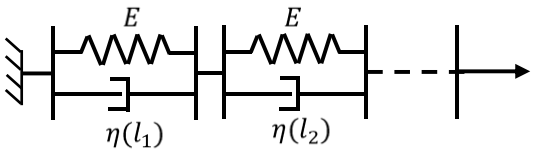

Figure 7. Viscoelasticity creep spectrum

The creep function can then be written as follows:

$$F(t) = \frac{1}{E}\int_0^{+\infty}\left(1 - e^{\frac{-\mathrm{E}\,t}{A\,\eta(l)}}\right) dl \quad (13)$$

which makes it possible to derive $\eta(l)$ from $F(t)$ (computation given in appendix B).

In the case of equation (9), with $E = E_s$, $\eta(l)$ is found equal to $\eta(l) = E_s\,\zeta(l)$, where $\zeta(l)$ is a non-dimensional function of l:

$$\zeta(l) = A\left(\Gamma(1-\beta)\right)^{\frac{1}{\beta}} l^{\frac{1}{\beta}} \quad (14)$$

~~1.2.3.~~2.2.3. "Juxtaposition" of the NLE + VE generic laws by series of 3-branch elements

In order to merge equations (8) and (9), a series of 3-branch elements is introducing, as illustrated in figure 8. To avoid duplicating the elastic components stemming from both NLE and VE spectra, the springs for each element are merged into a single one, whose value is set equal to E_s.

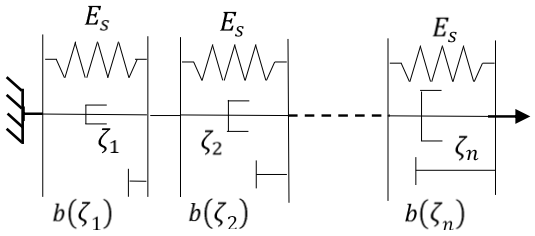

Figure 8. Series of 3-branch elements for CMA

In this model, the A parameter allows us to get a continuous transformation of the material from an unbound material at early age (small values for A) to an asphalt concrete material at cured state (after increase of $curing$ parameter and A value).

In equation (12), the l variable can be replaced by the ζ variable (equation (14)) to simplify the spectral representation, in which case the spectrum is characterized solely by the function $b(\zeta)$:

$$b(\zeta) = \left(\frac{\alpha}{\Gamma(1-\beta)}\right)^{\frac{\alpha}{\alpha-1}} \left(\frac{A}{\zeta}\right)^{\frac{\beta\alpha}{\alpha-1}} \quad (15)$$

From typical values for exponents α and β, i.e. 1.4 for α (derived from typical values of Boyce exponent n for granular materials) and 0.6 for β (the "h" exponent in the Huet model for HMA), the exponent $\frac{\beta\alpha}{\alpha-1}$ is found to be greater than 1, which makes $b(\zeta)$ monotonically decreasing from $+\infty$ to 0 for ζ varying from 0 to $+\infty$.

Now, by denoting $\varepsilon_\zeta(\zeta,t)$ as the "elementary deformation" of element ζ at time t, the total strain $\varepsilon(t)$ of the series is given by:

$$\varepsilon(t) = \frac{\beta}{\Gamma(1-\beta)A^\beta}\int_0^{+\infty}\frac{\varepsilon_\zeta(\zeta,t)}{\zeta^{1-\beta}}d\zeta \quad (16)$$

~~1.2.4.~~2.2.4. Modeling of curing

In this model, the parameter A is meant to account for the evolution of viscosity of CMA binders both with their curing state and the actual value of temperature θ. A first approach, which will be developed in future work from the on-going experimental campaign, will be to use the factorized form: $A(\theta, age\sout{,\{\theta\}}) = a(\theta\sout{(t)})\ v(age\sout{\{\theta\},t})$. As in the case of usual asphalt materials, the function $a(\theta)$ where θ is the actual value of temperature, is meant to account for the "immediate" change of viscoelastic properties of CMA with temperature. The higher θ, the softer the material. This function often called "function of translation in temperature" is generally taken close to the shape of a decreasing exponential and can be represented, for example, by the Williams-Landel-Ferry law [10]. Furthermore, it is generally found that the $a(\theta)$ function of asphalt concrete can be assimilated to the one of the bitumen used as binder [11]. In the present case $a(\theta)$, it will have to be checked if $a(\theta)$ can be deduced from the thermal behaviour of the bitumen used in the emulsion of CMA.

Beside $v(age)$ is meant to account for the curing of the material with its age since its manufacturing. Supposed to be equal to 0 just after manufacturing ($age = 0$), $v(age)$ increases with the material age. A priori $v(age)$ is itself a function of the temperature and moisture time histories $\{\theta\}: age \to \theta(age)$, $\{w\}: age \to w(age)$ that is $v(age) = \mathcal{F}(age, \{\theta\}, \{w\})$. One of our objectives starting from the results of our experimental campaign for which two different constant curing temperatures are used (20 and 35°C)

will be to identify the $\mathcal{F}$ function by taking inspiration from Doyle's work [12] which accounts for the acceleration of the curing process with temperature.

~~1.2.5.~~2.2.5. Calculation of the stress-strain relationship for the NLVE model

Let's now examine the response of the previous spectrum model to a given stress history, which constitutes a more direct problem than the inverse one (i.e. computation of stress for a given strain history), although the method described below can easily be adapted to the inverse case. This calculation is based on the numerical computation of the integral appearing in equation (16) and can be performed in three steps, namely:

(1) Discretisation of time into regular time steps Δt defining the times $t_i = i\,\Delta t$;
(2) For each time step $[t_i, t_{i+1}]$ and for any element of the spectrum, an incremental calculation of $\varepsilon_\zeta(\zeta, t_{i+1})$ in response to the given stress function and to the strain value of $\varepsilon_\zeta(\zeta, t_i)$ at time t_i is assumed to be known and stored in memory;
(3) Calculation of the integral in ζ by the trapezium rule, yielding the total strain response $\varepsilon(t_{i+1})$.

Step (2) is based on equations (17) to (19), which are exact for continuous and piecewise linear $\sigma(t)$ functions on intervals $[t_i, t_{i+1}]$. The equation to be used for any element ζ among equations (17), (18), (19) depends upon the open or close state of element at time t_i.

First case: Element ζ open at time t_i

Its evolution following time t_i is given by Equation (17):

$$\varepsilon_\zeta(\zeta, t) = \frac{\sigma_i}{E_s} + \frac{\dot{\sigma}_{i,i+1}}{E_s}(t - t_i - \zeta) + \left(\varepsilon_\zeta(\zeta, t_i) - \frac{\sigma_i}{E_s} + \frac{\dot{\sigma}_{i,i+1}}{E_s}\zeta\right) e^{\frac{-(t-t_i)}{\zeta}} \qquad (17)$$

where $\dot{\sigma}_{i,i+1} = \frac{\sigma_{i+1} - \sigma_i}{\Delta t}$ is the stress rate imposed between times t_i and t_{i+1}.

Two subcases can then again occur depending on the value of $\varepsilon_\zeta(\zeta, t)$ obtained at time t_{i+1} using equation (17):

(1) If $\varepsilon_\zeta(\zeta, t_{i+1}) \geq -b(\zeta)$, the element remains open throughout the time interval $[t_i, t_{i+1}]$ and the element deformation at time t_{i+1} is equal to $\varepsilon_\zeta(\zeta, t_{i+1})$.

(2) If $\varepsilon_\zeta(\zeta, t_{i+1}) < -b(\zeta)$, the element closes during the time interval (for a specific time value that does not need to be calculated in our algorithm), and the true element deformation at time t_{i+1} equals: $\varepsilon_\zeta(\zeta, t_{i+1}) = -b(\zeta)$.

Second case: Element ζ closed at time t_i

Now, the element will open between t_i and t_{i+1} only if the stress $\sigma(t)$ becomes smaller in absolute value terms than $E_s b(\zeta)$. Once again, two subcases are raised:

(1) If $\sigma(t_{i+1}) < -E_s b(\zeta)$, the element remains closed on the time interval $[t_i, t_{i+1}]$; the element deformation at time t_{i+1} is equal to $\varepsilon_\zeta(\zeta, t_{i+1}) = -b(\zeta)$.

(2) If $\sigma(t_{i+1}) \geq -E_s b(\zeta)$, the element opens at time t_{fo}, as defined by:

$$\mathrm{t_{fo}} = \mathrm{t_i} - \frac{\mathrm{E_s b(\zeta) + \sigma_i}}{\dot{\sigma}_{\mathrm{i,i+1}}} \tag{18}$$

The element deformation at time t_{i+1} is then given by:

$$\varepsilon_\zeta(\zeta, \mathrm{t_{i+1}}) = -\mathrm{b}(\zeta) + \frac{\dot{\sigma}_{\mathrm{i,i+1}}}{\mathrm{E_s}}(\mathrm{t_{i+1}} - \mathrm{t_{fo}} - \zeta) + \frac{\dot{\sigma}_{\mathrm{i,i+1}}}{\mathrm{E_s}}\zeta\, \mathrm{e}^{\frac{-(\mathrm{t}-\mathrm{t_i})}{\zeta}} \tag{19}$$

With these known values of $\varepsilon_\zeta(\zeta, t_{i+1})$, the total strain $\varepsilon(t_{i+1})$ of the spectrum can now be calculated by applying the trapezoidal rule to (16) and limiting the variation of ζ to the range $[0, \zeta_{max}]$ with $\zeta_{max} = \zeta_n$ being large enough. Then:

$$\varepsilon(t_{i+1}) \approx \frac{\beta}{\Gamma(1-\beta)A^\beta}\left(\int_0^{\zeta_1} \frac{\varepsilon_\zeta(\zeta, t_{i+1})}{\zeta^{1-\beta}} d\zeta + \sum_{j=1}^{j=n-1} \frac{(\zeta_{j+1} - \zeta_j)}{2}\left(\frac{\varepsilon_\zeta(\zeta_j, t_{i+1})}{\zeta_j^{1-\beta}} + \frac{\varepsilon_\zeta(\zeta_{j+1}, t_{i+1})}{\zeta_{j+1}^{1-\beta}}\right)\right) \tag{20}$$

To get an accurate precision, ζ_j values are taken into logarithmic progression between 10^{-15} and 10^5.

The first integral over the interval $[0; \zeta_1]$ is approximated by an analytical calculation to avoid the problem of singular integrand in $\zeta = 0$. For this, ζ_1 value is selected small enough with $b(\zeta)$ sufficiently high, being sure that all elements are open on the whole interval $[0, \zeta_1]$. Then:

$$\int_0^{\zeta_1} \frac{\varepsilon_\zeta(\zeta, t_{i+1})}{\zeta^{1-\beta}} d\zeta \approx \int_0^{\zeta_1} \frac{\frac{\sigma_i}{E_s} + \frac{\dot{\sigma}_{i,i+1}}{E_s}(t_{i+1} - t_i)}{\zeta^{1-\beta}} d\zeta = \left(\frac{\sigma_i}{E_s} + \frac{\dot{\sigma}_{i,i+1}}{E_s}(t_{i+1} - t_i) \right) \frac{\zeta_1^\beta}{\beta} \quad (21)$$

Finally, the entire procedure can easily be implemented into software for the step-by-step numerical computation of the material response $\varepsilon(t)$.

2.3. Examples of the strain-stress response of the 1D CMA model

A compressive sinusoidal test (fig. 9) was programmed using Visual Basic software to compute the strain response. Exponents β and α are taken equal to 0.6 and 1.4. The E_s parameter is defined by imposing $\varepsilon = 10^{-3}$ for $\sigma = 0.8\,MPa$ in equation (8), as typical values for unbound pavement materials. In these first calculations, which aim at representing a fresh material, A in equation (9) is taken equal to $2\ 10^{-2} s^{-1}$. This means that for a loading time of $2\ 10^{-2}$s and for a pressure of $1\ MPa$ which are typical orders of magnitude associated with traffic loads, the VE law would lead to strains in the order of 10^{-3}.

With this condition, figure 9 shows the strain obtained fort the CMA, as well as the NLE and VE curves calculated using the following relationships:

$$\text{Nonlinear elasticity: } \varepsilon(\sigma) = \left(\frac{\sigma}{E_s}\right)^{\frac{1}{\alpha}} \quad (22)$$

$$\text{Viscoelasticity: } \varepsilon(t) = F \otimes \dot{\sigma} \quad (23)$$

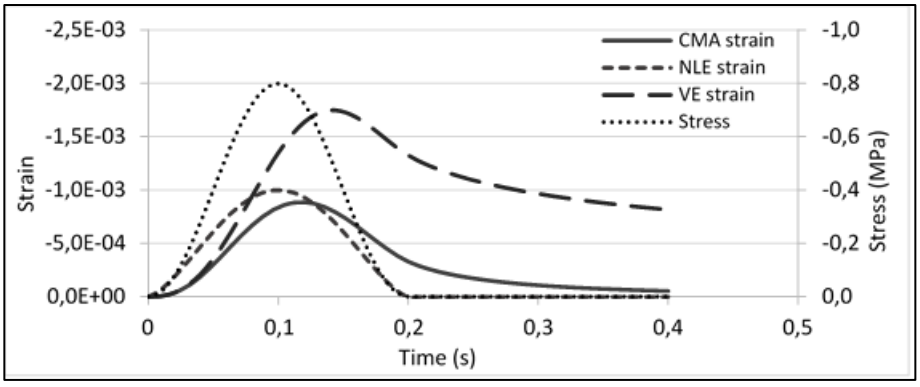

Figure 9. Strain response of CMA model to stress signal

As expected, the CMA strain curve looks equal to the VE deformation curve over a short time interval, but its maximum remains under the NLE curve. During the discharge, due to viscoelasticity, the CMA curve returns to zero well below the VE curve but more gradually than the NLE curve, which returns to zero at 0.2s.

~~3.~~4.First comparison between the model response and oedometric tests on CMA

~~3.1.~~4.1. Experimental tests on CMA

In parallel of this modelling work, an experimental campaign was managed to characterize the mechanical behaviour of CMA from fresh to cured state.

The tested material is a CMA (Table 1.), composed of basalt aggregate and a cationic emulsion with a binder content of 60% (including a 160/220 pen-grade bitumen).

Table 1. CMA formulation

Sieve (mm)	0.063	0.125	0.2	0.25	0.4	0.5	1	2	4	6.3	8	10	12.5	14	16
Passing (%)	7	9	11	13	16	19	28	43	62	73	79	86	95	99	100

Total water content (%)	Residual binder content (%)	Void ratio (%)
7.9	4.2	15

CMA has been compacted thanks to Duriez protocol. CMA specimens have been always kept in the Duriez molds for curing and mechanical testing. After compaction, CMA specimens have been stored in climatic chambers for three weeks under different controlled curing conditions (temperature of 20°C, 35°C and humidity ratio of 55%) to study the effect of these parameters on mechanical performance [13]. From time to time, the specimens will be shortly retrieved from the chambers to test them under cyclic oedometric conditions to measure their (complex) modulus. These tests are done at different frequencies (0.1, 1, 3, 6 and 10Hz) and temperatures in order to better assess their viscoelastic behaviour and possibly further characterize the curing parameter A of our model. Only mechanical performance measured at 20°C are shown in this article. A hundred of load cycles are applied on the whole life of the specimens to avoid

mechanical disturbance of the samples. To conduct these tests, a specific experimental device (fig. 10) was fully designed and manufactured specifically to study CMA mechanical behaviour.

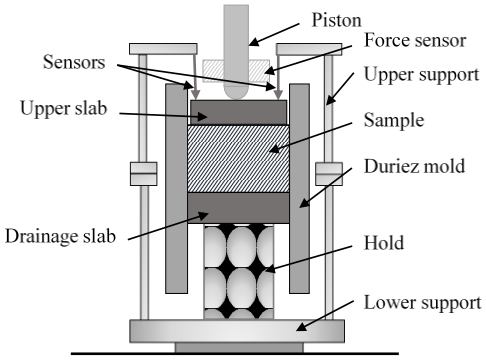

Figure 10. Device for the mechanical characterization test

The oedometric tests results presented in the following (fig. 11) were performed at different curing states at 20°C and 1 Hz for a sinusoidal stress of 0.4 MPa applied to the specimens. These first tests demonstrate a strong stiffening of the material with curing when comparing strain amplitude which decreases from $6{,}5\ 10^{-4}$ in the fresh state to $2{,}3\ 10^{-4}$ in the cured state.

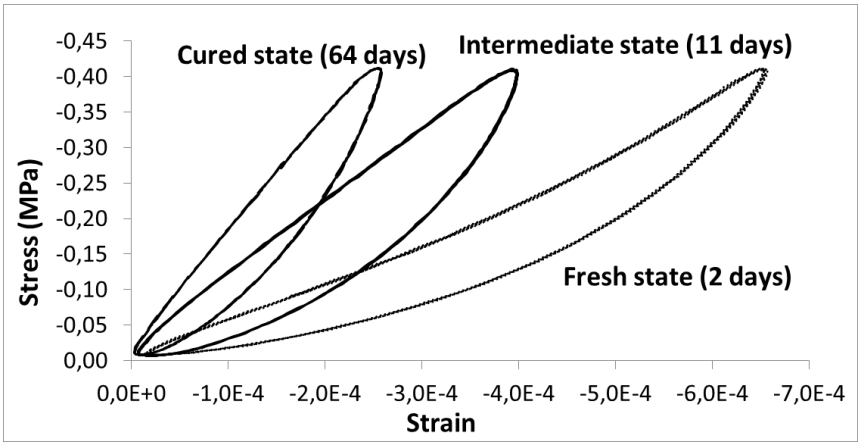

Figure 11. Experimental stress-strain cycles measured at 20°C on specimens cured at 35°C and 55% H.R

In the fresh state (2 days after manufacturing, compacting and curing at 35°C and 55% H.R), the CMA specimen displays at 20°C and 1 Hz an oedometric secant modulus

(calculated on the stabilized loading cycles) of 623 MPa. After 11 days and 64 days of curing, the modulus increases to 1038 MPa and 1761 MPa respectively. It can also be observed that with curing, the shape of the curves become less convex (fig. 11) which reflects the viscoelastic component increasing in the CMA behaviour. In the most cured state, the loading unloading loop even becomes elliptic.

~~3.2.~~4.2. Application of the CMA model for different values of "A"

To simulate these oedometric tests, a stress function $\sigma(t) = -0.4(1 - \cos \omega t)$ was run for few cycles in order to obtain the corresponding strain. The parameters β and α are kept equal to 0.6 and 1.4. The E_s parameter is defined by imposing $\varepsilon = 10^{-3}$ for the stress $\sigma = 0.4MPa$. The value of a is used to modify the model viscosity so as to observe the variation in material behaviour between the fresh and cured states (fig. 12 and 13). To be closed to the experimental results shown on figure 11, the parameter A is chosen as $2\ 10^{-3}s^{-1}$ (fresh state), $5\ 10^{-3}s^{-1}$ (intermediate state) and $10^{-2}s^{-1}$ (cured state).

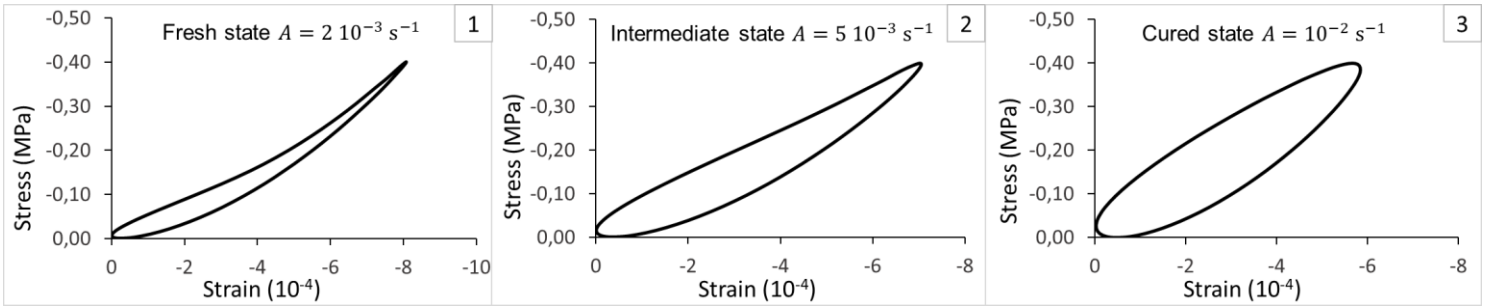

Figure 12. Simulation of three CMA loading cycles at the fresh state (1), at the intermediate state (2) and at the cured state (3)

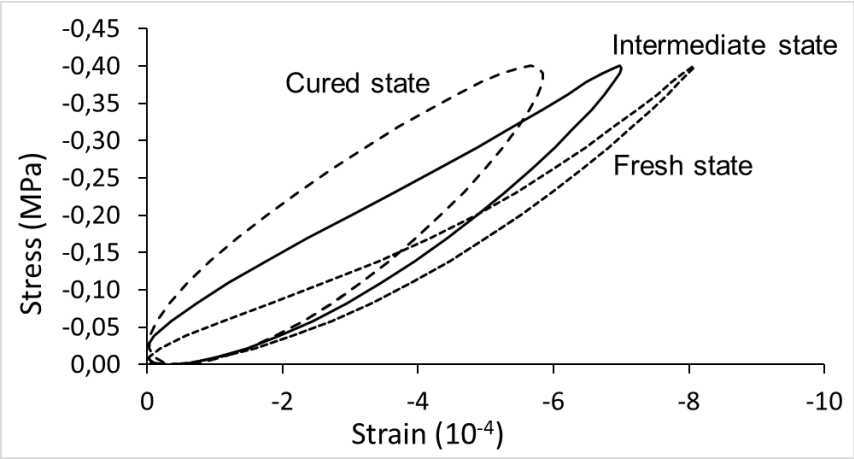

Figure 13. Simulation of 3 CMA loading cycles at the different states

Despite the fact that no specific attention has been given yet to optimise the fit between numerical and experimental curves, the qualitative comparison between figure 11 and figures 12 and 13 indicates that our 3 branches spectrum model looks promising to account for the evolutive behaviour (NLVE component) of CMA under curing.

~~4.~~5. Conclusion and outlook

This work has dealt with the need to develop a first-of-its-kind CMA constitutive model in order to introduce CMA as a structuring layer. The model is obtained as the juxtaposition of type Boyce model and a parabolic dashpot, using their spectral decomposition and the "curing function" $A(\theta, \text{age})$. Thus curing phenomenon is prone to be described by a dedicated function giving more and more weight with time to the viscous component. First comparisons between experimental results and numerical simulations show the relevance of the model to account for the CMA behaviour.

The experimental campaign launched in parallel to this work should make it possible to better define the values of the model parameters for an evolutive material. In particular, it is expected to be able to relate the function $A(\theta, \text{age})$ with the curing conditions. It is also planned to extend the model in 3D and to integrate it into a finite element software to compute the strain and stress fields induced in CMA pavement layers under traffic

and have a better knowledge of their mechanical behaviour over the pavement life. Further, damage criteria will have to be added on this basis.

~~5.~~6. Acknowledgements

The authors would like to thank Routes de France and l'Association Nationale de la Recherche et de la Technologie for funding this PHD and Jean Luc Geffard for his experimental contribution to this study.

~~6.~~7. References:

[1] Goyer, S., Dauvergne, M., Wendling, L., Fabre, J.C., de la Roche, C. & Gaudefroy, V. (2012). Environmental evaluation of gravel emulsion, Proceedings of International Symposium on Life Cycle Assessment and Construction – Civil engineering and buildings, Nantes, France.

[2] Serfass, J.-P.,De La Roche, C., Wendling, L., Gaudefroy, V. & Verhée, F. (2011) Emulsified asphalt mixes : Behaviour and design of grave-emulsion. Public private cooperation. Towards a complete design method. European roads review, N°19, RGRA, 1-4.

[3] Hornych, P., Gaudefroy, V., Geffard, J.L. & Goyer, S. (2009) Study of the mechanical behaviour of gravel-emulsions using triaxial tests, Proceedings of the 7th International RILEM Symposium on Advanced Testing and Characterization of Bituminous Materials, Rhodes, Greece.

[4] Serfass, J.-P., Poirier, J., Henrat, J., Carbonneau, X. (2004) Influence of curing on cold mix mechanical performance, Materials and Structures, Vol 37, 365-368

[5] Redelius, P., Östlund, J.A., & Soenen, H. (2016) Field experience of cold mix asphalt during 15 years, Road Materials and Pavement Design, 17:1, 223-242

[6] Wendling, L., Gaudefroy, V., Gaschet, J., Ollier, S. & Gallier, S. (2016) Evaluation of the compactability of bituminous emulsion mixes: experimental device and methodology, International Journal of Pavement Engineering, 17, 1, 71-80.

[7] Salomon, D. R. (2006). Asphalt emulsion technology (Transportation Research Circular E-C102), Transportation Research Board.

[8] Boyce, J.R. (1980). A non-linear model for the elastic behaviour of granular materials under repeated loading, Int. Symposium on Soils under Cyclic and Transient Loading, Swansea, U.K. 285-294.

[9] Huet, C. (1963). Comportement viscoélastique d'un matériau hydrocarboné. C.R. Acad. Sci. Paris 257, 1438-1442.

[10] Ferry, J.D., (1980) Viscoelastic Properties of Polymers, 3rd ed., John Wiley, New York.

[11] Boutin C., De La Roche C., Di Benedetto H., Ramond G., (1995) De la rhéologie du liant à celle de l'enrobé bitumineux, théorie de l'homogénéisation et validation expérimentale, Eurobitume Workshop, Bruxelles.

[12] Valentin, J. et al, (2014) Report on durability of cold-recycled mixes: moisture susceptibility, CEDR Call 2012: Recycling: Road construction in a post-fossil fuel society, CoRePaSol.
[13] Doyle, T., McNally, C., Gibney, A., Tabakovic, A., (2013) Developing maturity methods for the assessment of cold-mix bituminous materials, Construction and building materials, 38, 524-529.

Appendix A: Computation of the opening function $b(l)$

Let us examine the general computation of the opening function $b(l)$ linked to the nonlinear elastic relationship $\sigma(\varepsilon)$.

Let us start from equation (11) and figure 6. Considering the strain response to some given stress value σ, this integral (11) can be divided into two parts:

- the first one being related to the open elements for $0 \leq l \leq L(\sigma)$ where $L(\sigma)$ is the solution of the implicit equation:

$$b(L) = -\frac{\sigma}{E_s} \quad \text{(A1)}$$

- the second one being related to the closed elements for $L(\sigma) \leq l < +\infty$.

Thus:

$$\varepsilon(\sigma) = \frac{\sigma}{E_s} L(\sigma) - \int_{L(\sigma)}^{+\infty} b(l)\, dl \quad \text{(A2)}$$

Then by derivation with σ:

$$\frac{d\varepsilon}{d\sigma} = \frac{L(\sigma)}{E_s} \quad \text{(A3)}$$

Let us introduce the tangent flexibility modulus S defined by:

$$S(\sigma) = \frac{d\varepsilon}{d\sigma} \quad \text{(A4)}$$

Then:

$$S(\sigma) = \frac{L}{E_s} \quad \text{(A5)}$$

Then by elimination of σ between equations (A1) and (A5), it comes:

$$b(l) = -\frac{1}{E_s} S^{-1}\left(\frac{l}{E_s}\right) \quad \text{(A6)}$$

Let us apply this relationship to the particular case of the constitutive law (8). We have for this one:

$$\varepsilon = -\left(\frac{-\sigma}{E_s}\right)^{\frac{1}{\alpha}} \quad \text{(A7)}$$

and so for the flexibility modulus:

$$S(\sigma) = \frac{d\varepsilon}{d\sigma} = \left(\frac{1}{E_S}\right)^{\frac{1}{\alpha}} \frac{1}{\alpha} (-\sigma)^{\frac{1-\alpha}{\alpha}} \quad \text{(A8)}$$

Wherefrom:

$$S^{-1}(y) = -\left(\alpha E_S^{\frac{1}{\alpha}}\right)^{\frac{\alpha}{1-\alpha}} y^{\frac{\alpha}{1-\alpha}} \quad \text{(A9)}$$

And then:

$$b(l) = \frac{1}{(\alpha\, l)^{\frac{\alpha}{\alpha-1}}} \text{ with } \alpha > 1 \quad \text{(A10)}$$

Appendix B: Computation of the spectral function $\zeta(l)$ linked to the creep function $F(t)$

Lets us start from the relationship (13).

By time derivation, it comes:

$$\dot{F}(t) = \frac{1}{E}\int_0^{+\infty} \frac{1}{\zeta(l)} e^{\frac{-t}{\zeta(l)}} dl \quad \text{(B1)}$$

Let us note: $\frac{1}{\zeta(l)} = u$

and let us assume that $\zeta(l)$ is an increasing function, being equal to 0 for $l = 0$ and tending to $+\infty$ for $l \to +\infty$.

Then:

$$\dot{F}(t) = \frac{1}{E}\int_0^{+\infty} \frac{e^{-\mathrm{ut}}}{u} \frac{d\zeta^{-1}\left(\frac{1}{u}\right)}{du} du \quad \text{(B2)}$$

Then, it can be noticed that this relationship is similar to the Laplace transform of function $f(u)$:

$$\dot{F}(t) = TL[f(u)](\mathrm{t}) = \int_0^{+\infty} e^{-ut} f(u) du \quad \text{(B3)}$$

with:

$$f(u) = \frac{1}{E\,u} \frac{d\zeta^{-1}\left(\frac{1}{u}\right)}{du} \quad \text{(B4)}$$

Then by inverse transform:

$$\frac{1}{E\,u} \frac{d\zeta^{-1}\left(\frac{1}{u}\right)}{du} = TL^{-1}\left(\dot{F}(t)\right)(u) \quad \text{(B5)}$$

Wherefrom:

$$\frac{dl}{dv} = \frac{E}{v} TL^{-1}\left(\dot{F}(t)\right)\left(\frac{1}{v}\right) \quad \text{(B6)}$$

That is:

$$\frac{l}{E} = \int_0^{\zeta} \frac{TL^{-1}\left(\dot{F}(t)\right)\left(\frac{1}{v}\right)}{v} dv \quad \text{(B7)}$$

Finally, the requested equation for $\zeta(l)$ can be obtained by inverting this relationship.

Let us apply this computation to the particular case of the creep function (9). We have for this one with $B = \frac{1}{E_s}$:

$$\dot{F}(t) = \frac{\beta}{E_s A^\beta} \frac{1}{t^{1-\beta}} \quad \text{(B8)}$$

$$TL^{-1}\left(\dot{F}(t)\right)\left(\frac{1}{w}\right) = \frac{\beta}{E_s\, A^\beta} \frac{w^\beta}{\Gamma(1-\beta)} \quad \text{(B9)}$$

$$\frac{l}{E_s} = \int_0^\zeta \frac{TL^{-1}\left(\dot{F}(t)\right)\left(\frac{1}{w}\right)}{w}\, dw = \frac{1}{E_s\, A^\beta \Gamma(1-\beta)} \zeta^\beta \quad \text{(B10)}$$

And then:

$$\zeta(l) = A\, \Gamma(1-\beta)^{\frac{1}{\beta}}\, l^{\frac{1}{\beta}} \quad \text{(B11)}$$

Being given the inequality $\frac{1}{\beta} > 1$, it can be checked *a posteriori* that $\zeta(l)$ is equal to 0 for $l = 0$ and tends to $+\infty$ for $l \to +\infty$.